A Human-like Robot Hand and Arm with Fluidic Muscles: Modelling of a Muscle Driven Joint with an Antagonistic Setup

I. Boblan[1], J. Maschuw[2], D. Engelhardt[1], A. Schulz[3], H. Schwenk[1] and R. Bannasch[3], I. Rechenberg[1]

[1]Technische Universität Berlin, Fachgebiet Bionik & Evolutionstechnik, Ackerstr. 76, 13355 Berlin,
[2]Technische Universität Hamburg-Harburg, Arbeitsbereich Technische Informatik III,
[3]Fa. EvoLogics, F&E Labor Bionik, Ackerstr. 76, 13355 Berlin, Germany
boblan@bionik.tu-berlin.de

***Abstract*— Humanoid robots combine the optimized biological morphology and functionality of the real human with the mechanical constraints and limitations in the creation in a best way. This will be a trade-off at all times. The best biological solution of a detail is often simple in the function but too complex for the technical analogue.**

The paper deals with the idea of an artificial muscle, the quasi-static modelling of a single muscle, the physical modelling of an antagonistic muscle pair and the development of a handy linear model.

The first section introduces the idea of a bionically inspired robot. The second section gives a short introduction about fluidic muscle of the company FESTO[4] that is used in our robot. The third section shows three model approaches of the quasi-static behaviour of the fluidic muscle based on the statistically significant amount of measuring data. The Evolution Strategy is used to approximate the enormous amount of measuring data to handy compensation functions. Section 4 presents a physical modelling approach of an antagonistic muscle pair by use of established dynamic model equations and a possible reduction to a linear model. The last section gives a short outlook to the prospective work.

***Index Terms*—Bionik, Bionics, Control, Muscle, Modelling**

I. Introduction

Nature has been creating optimized individuals as well as morphology and physiology over a period of millions of years. They are adapted to the respective surrounding conditions und highly optimized to stay alive and to reproduce themselves.

In order to build humanoids we have to look at individuals in nature with the same proportions and environmental conditions and should not try to scale the joints of a beetle, for example, which were not designed to carry heavy weights. To keep in mind the scaling effects is one of the basic rules of the bionic development process.

The human as unrivalled role model requires the ability to run fast away from a danger. The same group of muscles has to sneak up to something as well. Depending on the scope of duty and performance of motion the muscles and the surrounding units (lever arm, connective tissue, tendons and ligaments) have to own the ability to adapt them. This adaptability of the sensor actuator system at simultaneous lightweight construction of the supporting body is considered to be a big challenge in the construction of a humanoid robot. To do the job perfect, the Humanoid should look like a human yet.

We will not look at industrial robots here, as they carry out rigid tasks among them-selves, or in contact with a technical environment. This field, called contact stability [1-3], has been widely investigated and has presented large problems for robotic manipulation tasks until today.

A humanoid muscle robot called “Zwei-Arm-Roboter V.4” in German (ZAR4) was developed during the last four years. The complete morphology and physiology is bionically inspired and based on a multitude of technical realisations of natural solutions. A detailed specification of the construction and functionality of the whole ZAR4 can be found in [4].

This paper is focused on the modelling of an artificial antagonistic fluidic muscle pair. In contrast to [5] the smaller fast switching valves with PWM signal excitation are used. The goal is to find a sufficient closed model for a specific operating range which is controllable and observable. Furthermore the model should maintain the availability for different types of muscles, external forces and should predict statements beyond the specific operating range too. For these reasons only the essence of a proper linear model of a fluidic muscle driven joint is considered.

[4] This project was supported by Dr. Werner Fischer and Univ. Prof. Axel Thallemer, FESTO AG & Co. KG.

II. Artificial Fluidic Muscle

The fluidic muscle of the company FESTO is used as actuator for the different versions of ZAR. The muscle consists of a tube which contracts under pressure and two appropriate aluminium end pieces which facilitate the connection of the incoming flow and provide the attachment point. The tube consists of the combination of an impervious, flexible tube and a covering of tightly woven threads in a diamond-shaped pattern. If the medium flows into the muscle and deforms the three-dimensional grid structure in the peripheral direction, a tensile force is generated in the axial direction. The grid structure is responsible for the characteristics of the muscle in particular the correlation of the internal pressure, the attached weight and the length of the muscle. The maximum contraction of a muscle without load is approx. 25% of the resting length. The following figure shows the design of a fluidic muscle.

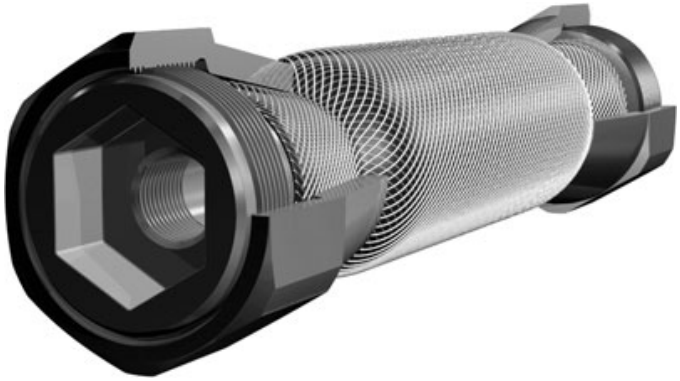

Fig. 1. The drawing above shows the structure of the fluidic muscle of the company FESTO.

The specification of the offered muscle can be found in [6]. The following details focus on the muscle type MAS20-200 – 20 mm diameter and 200 mm length L_0. The data of the ratio of air pressure P across length L_0 with different attached weights F of this muscle is shown in Figure 2 below.

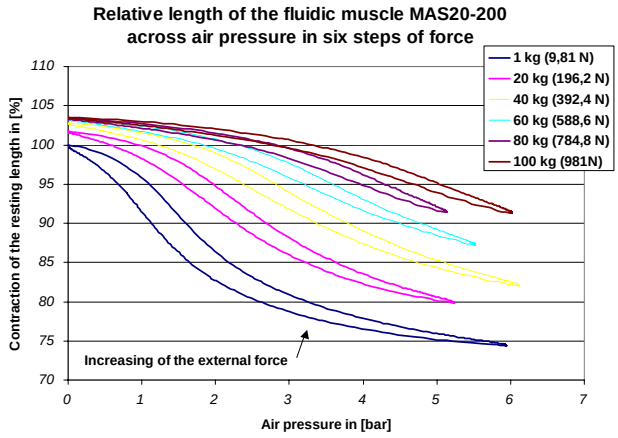

Fig. 2. The diagram above shows the measured ratio of the fluidic muscle MAS20-200 of air pressure across length and different attached weights.

All data is measured on test bed in our lab. The muscle stands in the upright position and one end is mounted on a base plate. A Dyneema® thread is connected to the other end of the muscle. The thread is guided across a pulley and is turned around by 180°. An angle transmitter as pulley axis measures the angle and therewith the elongation of the muscle. Possible weights can be attached on the hanging thread. The stretching of the Dyneema® thread is excluded from the real data. The acquired data is verified with the diagram of the specification of the muscle from the homepage of FESTO.

The curves in Figure 2 describe the ability of the muscle to shorten when inflating with air. The more weight has to be pulled the fewer the muscle shortens by constant air inside $L \propto 1/F$. The more the muscle can inflate the more shortening results by constant weight $L \propto P$. The maximum internal pressure $P_{\max}$ is specified with 6 bar but we use all types of muscles with approximately 8 bar and achieve a higher contraction.

It can be seen that each curve shows hysteresis behaviour between inflate (upper) branch and deflate (lower) branch. This lateral offset depends on the material of the muscle rubber tube (inertia) and is adjustable by the velocity of the in flowing air.

III. Quasi-Static Modelling of a Single Muscle

A quasi-static model of the muscle can be build if we disregard the dynamical aspects. The static characteristics of the proposed fluidic muscle can be combined to three static models.

The equation

$$V = g(L) \tag{1}$$

describes the geometrical coupling of the length and the volume which is qualified by the filament inside the muscle rubber tube.

The thermodynamic model of the change of state of an ideal gas can be described as in (2).

$$P\left(\frac{V}{m}\right)^{\chi} = const\,. \tag{2}$$

The equations (1) and (2) are picked up again in section IV *B* and *C* for the dynamical case.

The generated force of the actuator depending on the length and the inner pressure is given by the equation (3).

$$F = f(P, L)\,. \tag{3}$$

This main correlation will be carried out below.

If we assume that the inflowing air is sufficient slow (quasi-static), the hysteresis vanishes, then the in- and deflate branch are located on top of each other. The remained marginal

hysteresis can be disregarded simply because of the smallness compared to the elongation. The resulting curves in (3) can be modelled in different ways. Three different model approaches of the fluidic muscle are described below. All data fits in this paper were made using the Evolution Strategy developed by I. Rechenberg [7].

A. Power series model approach

The power series model gives the best possible data fit while suffering from a loss of comprehension of the tuned parameters and the loss of scalability to higher values in P and F. Furthermore is it not possible to transpose the resulted equation to F and P in closed form. It constitutes solely an abstract mathematical description of the measuring data.

The polynomial equation of the form

$$L(P,F) = P^n \cdot F^m \cdot x_{n,m} + P^{n-1} \cdot F^m \cdot x_{n-1,m} + \ldots + F \cdot x_{n-n,m-(m-1)} + x_{n-n,m-m} \quad (4)$$

is used to get the best possible data fit of the length L by different internal pressures P and outer forces F. The difference between the curve of the real data points and the power series can be calculated with the Matlab™ implemented function "polyfit2d". The function "polyfit2d" solves a quadratic error function by means of the simplex optimization for different powers in P and F. The following table shows the calculated differences.

TABLE I. CALCULATED DIFFERENCES BETWEEN REAL DATA AND THE USED POWER SERIES FOR F AND P TO DIFFERENT POWERS OF N AND M

F to the power of m → P to the power of n ↓	1	2	3	4
1	104,55	29,33	29,11	26,79
2	96,83	17,64	14,84	12,24
3	87,42	7,06	4,25	1,63e+4
4	87,39	6,90	3,84	2,25e+4
5	87,18	6,64	3,57	2,69e+4
6	87,17	6,63	3,62	7,27e+4
7	87,17	6,62	1,90e+4	8,28e+4

The map of the values in Table I gives a minimum for the powers of the series in F at 3 and in P at 5. The error between the real data and the power series relating to the resting length of the muscle is maximal 0.5 % and is equivalent to a length of 0.9 mm.

B. Spring or separation model approach

The idea for this type of model approach comes from the correlation that increasing the outer force leads to the increased muscle length and vice versa. Also important is the dependence of stiffness on the internal pressure.

The spring constant is define as follows:

$$\tilde{k} =: \frac{dF}{dL} = \frac{\partial F(L,P)}{\partial L} + \frac{\partial F}{\partial P} \cdot \frac{\partial P}{\partial L} \quad . \quad (5)$$

For a linear spring the term $\partial P/\partial L$ can be neglected which means that the internal pressure remains constant by pulling the muscle into the length. This simplification is well established and leads to a linear spring of the form

$$\bar{k} = \frac{F}{L(F) - L_0} \quad . \quad (6)$$

The problem of this form is, that due to the pressure driven contraction k would have positive and negative values. Especially the case with a certain force but no elongation causes a singularity in this formulation.

To avoid these possible singularities, (6) can be transferred as follows:

$$(F_{\max} - F) = \hat{k}(P,F) \cdot (L_{\max} - L) = f(L,P,F) \quad (7)$$

and constitutes rather a separation model approach. The constants $F_{\max}$ and $L_{\max}$ should be the maximum achievable values for F and L. This supported the physical context, while avoiding the singularity.

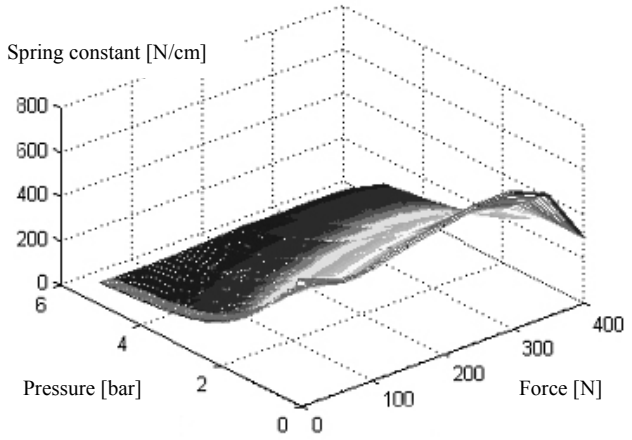

Fig. 3. The 3-D diagram above shows the calculated spring constant of muscle in different steps of external force and internal pressure.

In Figure 3 the linear spring constant is shown across different steps of external forces and internal pressures of the measured muscle. It can be discovered, that the calculated spring constant from the measuring data decreases when increasing the pressure. Remarkable is, that by increasing the external force the spring constant stays nearly constant with a small measurement error at 0 bar and 400 N.

The last observation opened the possibility to avoid a coupled system of equation. It is either possible to accept an error by use of an average value of the force or it is possible to identify a small range of force und define the force to a fix value so would the spring constant only depend on the pressure. The strain line could be adapted with hindsight anytime.

The simplified spring constant data points can be described by using an exponential function in shape similar to (8).

$$\hat{k}(P, F = const.) = x_1 + x_2\left(x_3 \cdot e^{\frac{-P}{x_3}}\right) \tag{8}$$

The parameter x_1 = 13.52 N/mm, x_2 = 42.28 N/mm bar and x_3 = 1.08 bar are identified by fit of the measuring data.

The error between the real data and the separation model relating to the resting length of the muscle in percent is maximal 2 % and is equivalent to a length of 3.5 mm.

The advantages of this model approach is the straightforwardness and scalability of the calculation equation, the simple transposing to the force *F* without using an equation solver and the physical motivation and therewith a benefit in imagination. A disadvantage is the increased fault tolerance in the considered working range.

C. Sine model approach

The sine model results from the specific examination of the group of curves in Figure 2. It can be seen that all curves feature a full or a half sine wave. And in addition each wave is rotated clockwise of about 45 %. To describe this behaviour a linear equation can be taken which describes the line between the start and the end point of a curve, shown in Fig. 4 left. This line is superposing with a sine function which describes the difference between the linear equation and the real data points, shown in Fig. 4 middle below.

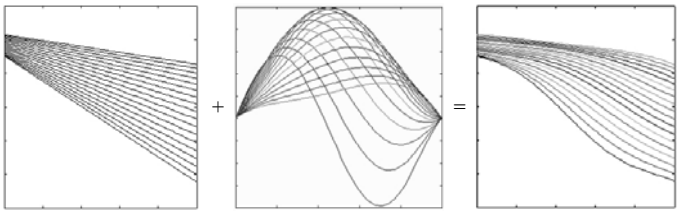

Fig. 4. The diagrams show a separation of the real data in Fig. 2 (right) in a linear (left) and a sine (middle) part.

Both parts are interconnect as follows:

$$L(P,F) = Lin(P,F) + Dif(P,F)\ . \tag{9}$$

1) "Lin" part

The linear part consists of a group of straight lines. These linear equations are displaced each other with increasing of the external force to greater length and smaller slope. The linear level equation of the form

$$Lin(P,F) = m(F)\cdot P + n(F) \tag{10}$$

describes this behaviour with $m(F)$ as slope and $n(F) = L(P = 0,F)$ as resting length, both depending on the external force *F*. The parameter *m* and *n* can be described as function of the external force *F*. The best function here is not the straight line but rather an exponential or sine function of the form

$$m^{I}(F) = n^{I}(F) = x_1^{I} - x_2^{I}\left(x_3^{I}\cdot e^{-\frac{F}{x_3^{I}}} - x_4^{I}\cdot e^{-\frac{F}{x_4^{I}}}\right) \quad or \tag{11}$$
$$m^{II}(F) = n^{II}(F) = x_1^{II}\cdot F - x_2^{II} + x_3^{II}\left(\sin\left(x_4^{II}\cdot F + x_5^{II}\right)\right).$$

The exponential function with index I is determined by four parameters which characterise the position in space. The parameter x_1^{I} moves the whole curve in the direction of the axis of ordinates *m* or *n*. The parameters x_2^{I}, x_3^{I} and x_4^{I} adjust two exponential bends within the curve one for small forces and one for larger forces. Two exponential terms are need if the data describe sigmoid behaviour otherwise satisfies one of.

The sine function with index II is determined by five parameters which characterise the position in space. In chronological order there are the rotation about zero, the displacement in *m* or *n*, the amplitude of the sine wave, the frequency of the sine wave and the displacement in *F*.

Both function approximations are similar. The exponential approach is derived from a time element of first or second order (PT1 or PT2).

2) "Dif" part

The difference between the group of straight lines and the real data, see Fig. 4 middle, can be described by a group of sine functions of the form below.

$$Dif(P,F) = x_1^{III}(F)\cdot P - x_2^{III}(F) + x_3^{III}(F)\cdot\sin\left(x_4^{III}(F)\cdot P + x_5^{III}(F)\right) \tag{12}$$

All parameters with index III in (12) are different functions of the force *F* again. The parameters $x_{1\text{-}5}^{III}$ in (12) describe the equation as well as the parameters with index II in (11).

If we look at the behaviour curves of the parameters depending of *F*, seen in Fig. 8 middle, it can be seen that the amplitude x_3^{III} first increases and after approximately 8 steps of force decreases again. The frequency described by the parameter x_4^{III} decreases at the same time. With this previous knowledge and with respect to the courses of the parameters in *F*, the function approximation of each parameter in (12) can be build just as well in (11) index II.

$$x_{1-5}^{III} = f(F) = m^{II}(F) = n^{II}(F) \tag{13}$$

Each parameter $x_{1\text{-}5}^{III}$ in (12) depends on five parameters described by equation (13). The system of five equations each with five unknown parameters described the difference part of (9) in a best way.

The maximum error is 0.9 % of the resting length or 1.7 mm. Remarkable is that in the error diagram the variation of the error across the force is noticeable greater than across the pressure. This fact is directly understandable because in our measuring method the steps of force are countable, one weight after another, while the steps of pressure are continuously changed by an adjustment valve. Consequently the dependence and the confidence across the pressure are higher as across the force.

A disadvantage of the sine model approach is the poor scalability for higher internal pressures und external forces. In reality the muscle does not show sine wave behaviour at most sigmoid behaviour, shown in Fig. 2. A second disadvantage is an increased calculation effort for the transposing to P or F.

D. Which model approach is the best?

The clearness of the model equation is an important point from the engineering point of view. Here the spring or separation approach has definitely prevailed. The accuracy of the calculation for this model is sufficient enough also in consideration of future muscle rubber compounds. The scalability of the spring or separation model equation beyond the measured scope is the best in the field. This is the determining factor for the choice of this model approach.

Both other model approaches are not subordinate with parameter values because of the clearness and briefness of the details and of the variety of muscle types.

IV. PHYSICAL MODELLING OF AN ANTAGONISTIC MUSCLE PAIR

To control an antagonistic pair of fluidic muscles not only the static behaviour but also the dynamic performance is required. To analyse the dynamic behaviour of an antagonistic fluidic muscle pair a second test bed was build which is similar to the muscle driven joints in our robot ZAR. The following Fig. 5 shows the test bed in the analysing process.

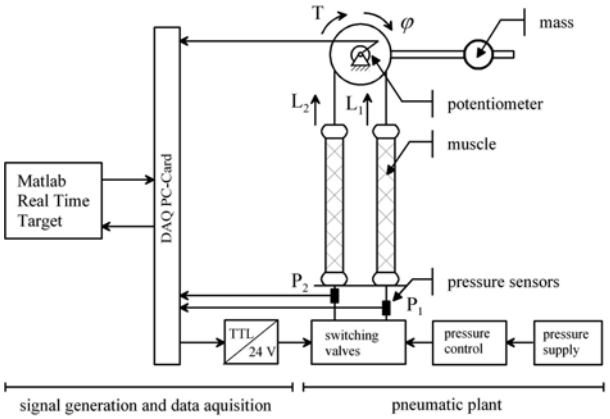

Fig. 5. The picture illustrates the muscle pair in the test environment.

The muscles are actuated with a maximum of 6 bar which are pulsed with two 3/2-port fast switching valves MHE2 from FESTO. The measured states are both pressures P_1 and P_2 each for one muscle and the muscle length. As pressure sensor the XFGM-3001 from Fujikura was used. The length is measured by a precision potentiometer MCP-40 from Megatron. It is driven by a Dyneema® thread which connects both muscle ends. On the axis of the pulley an extension arm is mounted which can hold different weights. This extension arm provides the possibility to stress the system with an outer disturbance. The toolbox "Real Time Windows Target" in MATLAB™ and a data acquisition cart PCI-6025E made by National Instruments do the signal processing.

If the connecting thread is tensed, both muscles pull against each other without rotating the joint. To connect the thread to the muscles, they get contracted by 50 % to reach the full working range.

On the one hand the physical fundamental equations are necessary to give information about the structural behaviour and the order of the modelled system and on the other hand to allow the differentiation of system states.

The following developed model is an analytic model because of any unknown parameters which have to be identified at a later date. The preliminary works of a McKibben muscle model in [8, 9] and of a FESTO muscle model in [5] are incorporated in the following details. The dynamic modelling of an antagonistic muscle pair can be divided into four different fields: fluid mechanics, kinematics, thermodynamics and mechanical principle of conservation of angular momentum.

A. Fluid mechanics

This part describes the context of the mass flow rate and the air pressure, the valve and the used fluid. The following equation (14) for the inlet holds under the condition that a proportional valve can be approximated by a fast switching valve drive by PWM signals.

$$\dot{m} = u \cdot A \sqrt{\frac{2\chi}{R \cdot T_{in}(\chi - 1)} P_{in}^2 \left[\left(\frac{P}{P_{in}} \right)^{\frac{2}{\chi}} - \left(\frac{P}{P_{in}} \right)^{\chi + \frac{2}{\chi}} \right]} \tag{14}$$

The parameter u is the pulse-width, A the area of valve opening, χ the polytrophic exponent identified in [5] to 1.26, R the specific gas constant, T_{in} the temperature of the supply, P_{in} the pressure of the supply and P the inner pressure of the muscle. For the behaviour of the outlet the same condition holds with negative sign. P_{in} has to be substituted by the internal pressure P and P by the environmental pressure P_{out}.

With prestressed muscles is it possible to neglect the difference between inlet and outlet in (14). For a linear approximation the operating point is indexed by subscript 0. The radicand in (14) can be substitute by $\Phi(P_0)$ so that:

$$\dot{m} = \pm u \cdot A \cdot \Phi(P_0). \tag{15}$$

B. Kinematics

For the description of the muscle volume, a functional relation (16) between volume and length was assumed in [8]. For the FESTO muscle with a similar structure, this assumption could also lead to good results. But due to the apparently different designs of the muscle meshes, this cannot be said definitely and cannot be postulated as a basic principle.

$$V = g(L) \quad and \quad \dot{V} = g'(L) \cdot \dot{L} \tag{16}$$

The function $g(L)$ in (16) have to be identified in the future.

Close to the operating point $L = L_0$ the condition (17) holds.

$$V = V_0 + g'(L_0)\cdot \Delta l \quad and \quad \dot{V} = g'(L_0)\cdot \Delta \dot{l} \tag{17}$$

C. Thermodynamics

The thermodynamic part of the muscle modelling describes the context of the pressure rate P' proportional to the mass flow rate m' and the change in volume V'. The relation

$$P_1 \cdot V_1^{\chi} = P_2 \cdot V_2^{\chi} \quad with \quad P \cdot v = R \cdot T \ and \ v = \frac{V}{m} \tag{18}$$

is used to describe the thermodynamic properties. The parameter P is the pressure inside the muscle, V the inner volume, χ the polytrophic exponent, R the specific gas constant, T the gas temperature and v the ratio of volume V and mass m. The derivative with respect to time of (18) leads to

$$\dot{P} = \chi \cdot P\left(\frac{\dot{m}}{m} - \frac{\dot{V}}{V}\right). \tag{19}$$

To obtain the relation between the rate of pressure P' and the length of the muscle L directly, the volume V in (19) can be substituted by the kinematics relations in (16).

$$\dot{P} = \chi \cdot P_0\left(\frac{\dot{m}}{m_0} - \frac{g'(L_0)\cdot \Delta \dot{l}}{V_0}\right). \tag{20}$$

D. Conservation of angular momentum

The conservation of angular momentum combines the dynamics of both muscles to the dynamics of an antagonistic muscle pair, shown in Fig. 5.

$$J \cdot \ddot{\varphi} = -\delta \cdot \dot{\varphi} + (F_1 - F_2)r + M \cdot g \cdot a \cdot \cos(\varphi) + T\ . \tag{21}$$

The parameter J is the moment of inertia, φ the angle which corresponds to the change of length of the muscles, δ the coefficient for viscous friction, F the produced force of the muscles, r the radius of the connecting pulley, M the mass of the extension arm, g the acceleration due to gravity and T the load moment on the axle of the pulley. The nonlinear equation (21) can be linearised around an expedient operating point and yields to

$$J \cdot \ddot{\varphi} = -\delta \cdot \dot{\varphi} + (F_1 - F_2)r + T\ . \tag{22}$$

The torque due to the weight is compensated by the increased stress of one muscle and the decreased stress of the other muscle. The basic condition is that the connecting Dyneema® thread is always tensed what leads to the following stringent condition

$$\Delta l_1 = -\Delta l_2 = \varphi \cdot r\ . \tag{23}$$

The forces in (22) can be described by the relation in (3). The physical relation of the quantities F, P and L to each other is only approximately known. For the real physical model of the muscle the detailed build-up and rubber compound has to be known in bonding with the embedded braiding.

The model approach using the energy balance for a McKibben muscle in [8] is not applicable because of the unmodelled elastic deformation of the muscle membrane. The McKibben muscle always has to be prestressed in contrast to the FESTO muscle which works without external force too.

The approach via quasi-static characteristic curves in section III, also favoured in [5], is a first approximation and is not scalable to other types of muscles. The linearisation of (3) leads to

$$F(\Delta p, \Delta l) = f(P_0, L_0) + f_{\Delta l}(P_0, L_0)\Delta l + f_{\Delta p}(P_0, L_0)\Delta p\ . \tag{24}$$

Equations built by fitting of measuring data as it has been done in section III cannot give any information about the first differentiation of the equation of the real physical model. The fitting functions are used to approximate the measuring data at best and not to describe the physical background of the data.

The four fields mentioned above describe the dynamic model of an antagonistic muscle pair analytically. Solely the just mentioned relations in (3) and in (16) have to be acquired by measuring.

The equations (3), (14), (16), (19) for each muscle and (21) and (23) yield to a nonlinear model of the motion of the antagonistic fluidic muscle pair.

$$\begin{bmatrix} \varphi \\ \dot{\varphi} \\ P_1 \\ P_2 \\ m_1 \\ m_2 \end{bmatrix}' = \begin{bmatrix} \dot{\varphi} \\ 1/J\left(-\delta\dot{\varphi} + Mga\cos(\varphi) + (f_1 - f_2)r + T\right) \\ \chi P_1\left(\frac{\dot{m}_1}{m_1} - \frac{g_1'(\varphi)\dot{\varphi}}{g_1(\varphi)}\right) \\ \chi P_2\left(\frac{\dot{m}_2}{m_2} - \frac{g_2'(\varphi)\dot{\varphi}}{g_2(\varphi)}\right) \\ uA\Phi_1(P_1) \\ -uA\Phi_2(P_2) \end{bmatrix} \tag{25}$$

The variables f_1, f_2 stands for $f_1 = f_1(P_1,\varphi)$ and $f_2 = f_2(P_2,\varphi)$. Six states are essential to the description of the model dynamics. The function f_1 and f_2 and respectively g_1 and g_2 merely differ in the dependence on φ given by (23). The directions of the mass flow rate determine the use of Φ_1 or Φ_2.

The linear equations (15), (17), (20) and (24) for each muscle and (22) yield to a state space model around the equilibrium point $\Delta l = 0$, shown in Fig. 5. In this point it can be assumed that for small masses the states of both muscles are equal, $m_{10} = m_{20} = m_0$, $V_{10} = V_{20} = V_0$, $P_{10} = P_{20} = P_0$ and $L_{10} = L_{20} = L_0$. With $\Delta^2 p = \Delta p_1 - \Delta p_2$ (22) can be rewritten as

$$\ddot{\varphi} = \frac{1}{J}\left(-\delta\cdot\dot{\varphi} + \left(f_{\Delta p}\cdot\Delta^2 p - 2 f_{\Delta l}\cdot r\cdot\varphi\right)r\right). \tag{26}$$

where the pressure difference is

$$\Delta^2\dot{p} = 2\chi P_0\left(\frac{A\cdot\Phi(P_0)}{m_0}u + \frac{g'(L_0)r}{V_0}\dot{\varphi}\right). \tag{27}$$

According to this the motion around the equilibrium point can be described as differential equation of third order.

$$\begin{bmatrix}\varphi\\ \dot{\varphi}\\ \Delta^2 p\end{bmatrix}' = \begin{bmatrix}0 & 1 & 0\\ -\frac{2 f_{\Delta l} r^2}{J} & -\frac{\delta}{J} & \frac{f_{\Delta p} r}{J}\\ 0 & 2\chi\frac{P_0 g'(L_0)r}{V_0} & 0\end{bmatrix}\begin{bmatrix}\varphi\\ \dot{\varphi}\\ \Delta^2 p\end{bmatrix} + \begin{bmatrix}0\\ 0\\ \frac{2\chi P_0 A\Phi(P_0)}{m_0}\end{bmatrix}u + \begin{bmatrix}0\\ \frac{1}{J}\\ 0\end{bmatrix}T. \tag{28}$$

In case of a possible equilibrium state $\varphi' = \varphi'' = \Delta^2 p = 0$ and $u = T = 0$ the equilibrium positions follow to

$$\frac{\varphi}{\Delta^2 p} = \frac{f_{\Delta p}}{2 f_{\Delta l}\cdot r}. \tag{29}$$

For this linear equation system the controllability and observability can be analysed by the criterion of Kalman without the determination of the parameters.

$$W = \left[B, AB, A^2 B\right] = \begin{bmatrix}0 & 0 & \xi_3\xi_5\\ 0 & \xi_3\xi_5 & -\xi_2\xi_3\xi_5\\ \xi_5 & 0 & \xi_3\xi_4\xi_5\end{bmatrix} \tag{30}$$

For $\xi_{1\text{-}5} \neq 0$, in the abstract case, the matrix W has full rank of three and the complete controllability is thus given.

The observability matrix M

$$M = \left[C, CA, CA^2\right] = \begin{bmatrix}1 & 0 & 0\\ 0 & 1 & 0\\ -\xi_1 & -\xi_2 & \xi_3\end{bmatrix} \; with \; C = [1,0,0] \tag{31}$$

has full rank even if only the angle is measured under the condition of $\xi_{1\text{-}3} \neq 0$.

The given complete controllability and observability for a system is a quantity for the quality of the future control.

V. Outlook

This paper deals with the static modelling on a fluidic muscle and the physical modelling of the muscle itself and as part of an antagonistic muscle pair. The derived nonlinear analytical model and hence the extracted handy linear model constitute the basis for future control strategies. The used model setup is part in each of the joints of our humanoid robot ZAR. With the physical model and thus a prediction of the robots dynamics it is possible to control the motion in the whole kinematics range. The derived model enables compliant and fast motions in predetermined way.

The next step is to develop different control strategies which are tested at present.

References

[1] Šurdiloviæ, D.T., *Synthesis of Robust Compliance Control Algorithms for Industrial Robots and Advanced Interaction Systems*, in *Mechanical Engineering Faculty*. 2002, University in Niš. p. 475.

[2] Okada, M., Y. Nakamura, and S. Ban. *Design of Programmable Passive Compliance Shoulder Mechanism*. in *Proceedings of the 2001 IEEE Int. Conference on Robotics & Automation*. 2001. Seoul, Korea.

[3] Rocco, P., G. Ferretti, and G. Magnani, *Implicit Force Control for Industrial Robots in Contact with Stiff Surfaces.* Automatica, 1997. **33**(No.11): p. 2041-2047.

[4] Boblan, I., et al., *A Human-like Robot Hand and Arm with Fluidic Muscles: Biologically Inspired Construction and Functionality*, in *Embodied Artificial Intelligence*, F. Iida, et al., Editors. 2004, Springer-Verlag: Berlin Heidelberg. p. 160-179.

[5] Hildebrandt, A., et al., *A Flatness Based Design for Tracking Control of Pneumatic Muscle Actuators.* Seventh Int. Conference on Control, Automation, Robotics and Vision (ICARCV), 2002: p. 1156-1161.

[6] FESTO, *Fluidic Muscle MAS,* http://www.festo.com/INetDomino/coorp_sites/en/1b433eb8d078cbd2c1256c7e0039bf43.htm. 2005, FESTO AG & Co. KG.

[7] Rechenberg, I., *Evolutionsstrategie '94*. 1994: fromman-holzboog. 434.

[8] Chou, C.-P., *Measurement and Modeling of McKibben Pneumatic Artificial Muscles*. 1996, Department of Electrical Engineering, FT-10: Washington 98195, Seattle. p. 22.

[9] Colbrunn, R.W., *Design and Control of a Robotic Leg with Braided Pneumatic Actuators*, in *Department of Mechanical and Aerospace Engineering*. 2000, Case Western Reserve University. p. 141.

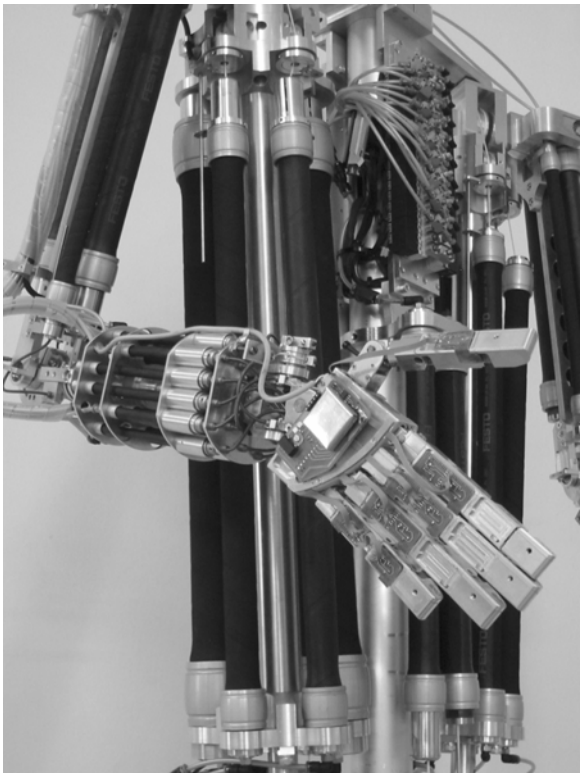

Fig. 6. The anthropomorphic muscle robot ZAR4 is shown.